AAS 19-534

REAL-TIME TELESCOPE TASKING FOR CUSTODY AND ANOMALY RESOLUTION USING JUDICIAL EVIDENTIAL REASONING

Daniel Aguilar Marsillach [*], Shahzad Virani [†], Marcus J. Holzinger [‡], Moses W. Chan [§] and Prakash P. Shenoy [¶]

As the near-Earth space object population increases in size, SSA sensor tasking becomes more complex. Most forms of tasking focus on covariance minimization, information maximization or catalog maintenance. Limited work has been done on tactical hypothesis-based sensor tasking, which resolves the problem from a decision-making perspective. Hypotheses can be formulated resolved using Dempster-Shafer evidential reasoning. Previous work lead to the formulation of Judicial Evidential Reasoning, resulting in optimal and unbiased hypothesis resolution under time constraints. This paper focuses on applying the Judicial Evidential Reasoning algorithm to resolve the anomaly and custody hypotheses of space objects using a telescope. The contributions in this paper include formulating new evidence to hypothesis belief mappings in Dempster-Shafer theory, incorporating a reachability set search action, and implementing the algorithm in real-time for a narrow field-of-view telescope.

INTRODUCTION

There is a warranted concern for the safety of current and future space-assets as a result of an increasing number of Earth-orbiting objects. To guarantee the safety of future space missions and operations, for commercial or scientific reasons, it is imperative to understand and predict how resident space object states are evolving.[1] This is part of the goal of space situational awareness (SSA). It is essential that capabilities to detect and track space objects using both ground and space-based instrumentation are improved. An important goal of which is minimizing conjunction events between current resident space objects (RSOs).

Currently, there are a limited number of optical and radar ground sensors that are used to update state estimates of the RSO population. Information about the current state of the environment is extracted by taking measurements (sensing) and combining them with physics-based models. However, due to an increasing RSO population, maintaining an understanding of the orbital environment is becoming increasingly challenging due to limited time and resources. As a result, an

[*] PhD Student, Ann & H.J. Smead Aerospace Engineering Sciences, University of Colorado Boulder, 2598 Colorado Ave, Boulder, CO 80309

[†] PhD Student, Ann & H.J. Smead Aerospace Engineering Sciences, University of Colorado Boulder, 2598 Colorado Ave, Boulder, CO 80309

[‡] Associate Professor, Ann & H.J. Smead Aerospace Engineering Sciences, University of Colorado Boulder, 2598 Colorado Ave, Boulder, CO 80309

[§] Technical Fellow, Lockheed Martin Space Systems, Sunnyvale, CA 94089

[¶] Distinguished Professor, School of Business, University of Kansas, 1654 Naismith Drive, Lawrence, KS 66045

area of improvement lies in the tasking of sensors for SSA. This boils down to resource utilization for both ground and space-based observers. Previous tasking methodologies are aimed at extracting high-quality six-dimensional state estimates through covariance minimization or Fisher information maximization.[2,3] This allows operators to predict the dynamics of RSOs with greater accuracy and reliability.[4] Covariance minimization techniques are essential for accumulating data to resolve unknown unknowns. However, how one uses a suite of sensors to resolve known unknowns is of interest as it links SSA hypotheses directly to sensor management. How sensors are used to track known targets in place of searching for new ones is non-trivial.[5] This paper focuses on the tasking problem from a hypothesis centric perspective using evidential reasoning techniques and ignores active searching for unknown RSOs.

Past work has been completed using Dempster-Shafer (DS) theory for tasking or decision-making problems. DS theory is one of many theories of belief functions and lies at the core of this work. Hypotheses can be formulated mathematically using the frame of discernment, which is essentially an outcome space. Compared to other belief function theories, such as Bayesian probability theory, DS theory is more expressive when modeling ignorance (ambiguity) in the state space of a random variable, as belief can be given to subsets of the frame of discernment. In Bayesian theory, declaring complete uncertainty and having an uninformative prior are both modeled as a uniform distribution of equally-likely propositions.[6] DS theory allows one to model these two differing cases unambiguously, which can be important for decision-makers acting on resulting information. Though many evidence-gathering approaches prioritize maintaining low overall state covariance, it is not immediately clear how this affects situational awareness or aids in decision-making. This motivated an approach that considers decision-making objectives as hypotheses that can be investigated by evidence-gathering actions.[7]

One such tasking scheme focused on minimizing the ignorance or ambiguity in the proposed frame of discernment, which drives the system to resolve hypotheses. This methodology was applied to an SSA scenario where custody of RSOs is maintained.[8] More recently, Jaunzemis et al. developed a general decision-making algorithm that optimally selects actions to reduce total system entropy.[7] Using adversarial optimization, action sequences that are optimal to specific propositions of a frame of discernment are combined to form a single hybrid action sequence. This paper extends the capabilities of Judicial Evidential Reasoning (JER) and applies it to a real telescope system.

Two indvidual hypotheses are considered for each RSO. The first hypothesis relates to maintaining custody of RSOs. The second one, denoted the anomaly hypothesis, requires determining whether or not an RSO is in its nominal orbit. Any deviation from the nominal orbit provides evidence of unknown or unexpected dynamics, which can be caused by unmodeled perturbations or maneuvers. This hypothesis is particularly important as RSOs in anomalous orbits can compromise the safety of other active assets. This work presents the results obtained when implementing the JER algorithm on the Georgia Tech - Space Object Research Telescope (GT-SORT) to resolve the listed hypotheses using optical data in real-time.

A lack of custody requires a search methodology for re-acquisition. As such, a search strategy is incorporated into this version of JER that iteratively observes volumes of state space near the object's nominal orbit. It is assumed that the maximum deviation with respect to this trajectory is related to the object's reachable set. This set can be constructed using optimal control techniques and highlights the maximal distance in $\mathbb{R}^n$ that an object can travel, placing a maximum bound on the object's deviation from a nominal trajectory. This constrains the search region. JER uses DS theory combined with estimation techniques to form a tasking algorithm that is able to evaluate

and execute action sequences for optimal hypothesis resolution. Hypotheses are posed using natural language and can be general in formulation, as long as there is an ability to map evidence to them. In some sense, JER allows a user to specify and define how much evidence is required to appropriately resolve a hypothesis.

This paper contains a number of contributions relating to the application and extension of the JER scheduling algorithm for SSA. First, reachability search actions are introduced such that the algorithm is able to survey portions of state-space to detect and track RSOs whose custody is not maintained. Second, new evidence to hypothesis belief mappings are formulated that result in an improved way of quantifying evidence. Lastly, the algorithm is interfaced with existing observatory hardware for the purpose of an empirical validation.

BACKGROUND THEORY

Dempster-Shafer Evidential Reasoning

An advantage of DS theory is its ability for reasoning with epistemic uncertainties, as one can model degrees of support for a particular proposition, given a piece of evidence. This can simplify decision-making by using Dempster's combination rule for aggregating independent pieces of evidence.[9] The theory allows one to pose and resolve a hypothesis mathematically as well as model complete ambiguity and equally likely propositions differently. Moreover, Bayesian probability theory is embedded in Dempster-Shafer theory as a special case, and can be interpreted as a generalization of that theory.[9]

The available state space of a variable is denoted by the set Θ called the frame of discernment. The elements of the power set of Θ, 2^Θ, or the set of all subsets, are referred to as propositions. By definition, the allowable state variables in the frame of discernment have to be mutually exclusive and collectively exhaustive, implying that only one element of the frame of discernment can be true.

For a given frame of discernment, Θ, the basic probability assignment (BPA) function m assigns degrees of belief or support to particular elements of the power set 2^Θ and is defined as:

$$m : 2^\Theta \mapsto [0, 1] \tag{1}$$

$$m(\emptyset) = 0 \tag{2}$$

$$\sum_{a \in 2^\Theta} m(a) = 1 \tag{3}$$

The constraint in Eqn. 3 enforces the mutually exclusive and collectively exhaustive property. The quantity $m(a)$ is the basic probability mass of set a, and is interpreted as the belief assigned exactly to a (not its subsets). Additionally, Eqn. 2 enforces that no belief is committed to the null set.

Two BPAs m_1 and m_2, representing distinct pieces of evidence, can be combined to form a new aggregate BPA $m_1 \oplus m_2$ using Dempster's combination rule:[11]

$$(m_1 \oplus m_2)(a) = K^{-1} \sum_{b_1, b_2 \in 2^\Theta : b_1 \cap b_2 = a} m_1(b_1) m_2(b_2) \tag{4}$$

where K is a normalization constant given by:

$$K = 1 - \sum_{b_1, b_2 \in 2^\Theta : b_1 \cap b_2 = \emptyset} m_1(b_1) m_2(b_2) \tag{5}$$

Dempster's rule of combination yields a BPA that updates the belief states in the frame of discernment. If distinct pieces of evidence agree, a new BPA is created that reflects more support for a particular set of propositions. If $K = 0$, then BPAs m_1 and m_2 are said to be in total conflict, and the evidence cannot be combined. If $K = 1$ then BPAs m_1 and m_2 are non-conflicting. This normalizing constant is used to account for any belief given to the null set.

Additionally, the plausibility function, denoted $Pl_m(x)$ corresponding to BPA m, is defined as:

$$Pl_m(a) = \sum_{b \in 2^\Theta : b \cap a \neq \emptyset} m(b) \tag{6}$$

for all $a \in 2^\Theta$. The plausibility of a is the sum of the belief masses for propositions that do not explicitly refute a, and can be interpreted as an upper bound on the possibility that a is true.

Moreover, Cobb and Shenoy defined a way to transform Dempster-Shafer belief functions to Bayesian probability ones, through the plausibility transformation.[12] This is motivated by the fact that decision-making criteria is simpler in Bayesian theory. Though DS theory is excellent at combining pieces of information, it comes with the limitation of not having a specific guide on how to make decisions. Other transform types include the pignistic probability transform.[13] The plausibility transform thus allows one to use Bayesian decision-making criteria with DS theoretic belief functions. This transformation is defined as:

$$Pr_{pl_m}(x) = \widetilde{K}^{-1} Pl_m(x) \tag{7}$$

where

$$\widetilde{K} = \sum_{x \in \Theta} Pl_m(x) \tag{8}$$

Judicial Evidential Reasoning

Fundamentally, JER selects actions that best resolve a set of hypotheses. The algorithm iteratively evaluates action paths that gather multiple pieces of evidence to resolve hypotheses to a reasonable tolerance. Since frames of discernment are mutually exclusive and collectively exhaustive, JER attempts to find the true state variable by minimizing a defined cost function. One potential cost function is entropy, which is a measure of uncertainty in the state space. Many entropy definitions are summarized in Jiroušek and Shenoy's prior work.[14] One such definition is Jiroušek-Shenoy (J-S) entropy, which is interpreted as a measure of total uncertainty in a BPA. This new definition combines Shannon and Dubois-Prade entropy to capture both conflict (uncertainty) and

non-specificity (ambiguity).[14] Low conflict means significant belief mass is attributed to a singleton proposition. Non-specificity captures mass given to subsets of the frame of discernment with non-singleton propositions.

J-S entropy is maximum for vacuous BPAs that represent complete ambiguity or ignorance. This occurs when all of the belief mass is given to the frame of discernment such that $m(\Theta) = 1$, representing a complete lack of knowledge of which element $a \in \Theta$ is true. Minimizing J-S entropy is directly equivalent to identifying the true proposition in a frame of discernment. J-S entropy then becomes an appropriate measure, or objective function, to be minimized for the purposes of hypothesis resolution. However, obtaining necessary optimality conditions is difficult due to the high-dimensional, mixed-integer and nonlinear properties of the problem. As such, a computational approach is adopted where potential outcomes, due to actions, are scored and chosen to task a sensor.

JER seeks to resolve a set of hypotheses, $\Theta = \{\Theta_1, ..., \Theta_h\}$, where Θ_h is an individual hypothesis of size $|\Theta_h|$. A discrete-time sequence, $t = [t_0, t_1, ..., t_f]$, is considered at which sensor actions can be taken. An action at time t_i, for a particular sensor j, is denoted $a_{i,j}$. The sequence $\mathcal{A}_s = [a_{1,s}, a_{2,s}, ..., a_{f,s}]$ represents a discrete-time action sequence for sensor s over the time-horizon, where s is the sensor index. Additionally, each sensor has a variable number of possible actions $|a_{i,j}|$ at a particular time index. The set containing all the possible action sequences for a single sensor s is denoted $\alpha_s = [\mathcal{A}_1, ..., \mathcal{A}_p]$, where p is the number of unique action sequences. When m sensors are considered, the full set of available actions is computed via Cartesian products:

$$\alpha = \alpha_1 \times \alpha_2 \times \cdots \times \alpha_m \tag{9}$$

In this paper, actions are abstracted as deliberate choices for a sensor to observe a particular RSO. If there is a single ground station, and 5 RSOs are visible for the entire time-horizon, then, the sensor has 5 available actions at each moment in time. In reality, different RSOs are visible to different ground stations at different times. This is taken into account when computing available action sequences.

The objective is to minimize the J-S entropy, H_{JS}, of all hypotheses. The weights, w_h, specify the priority or preference for resolving a particular hypothesis h. Mathematically, the problem is:

$$\alpha^* = \arg\min_{\alpha} \sum_{h=1}^{|\Theta|} w_h H_{JS}, \tag{10}$$

where α contains the decision variables (sequences) over which the optimization occurs. If only one sensor is considered, then $\alpha = \alpha_1$. If there are n RSOs of interest, then the action at time t_i for a given sensor j, is a function of the following form:

$$a_{i,j} = f(\mathbf{x}_{rso}(t), \mathbf{x}_{gs}(t), P_d), \tag{11}$$

where $\mathbf{x}_{rso}, \mathbf{x}_{gs} \in \mathbb{R}^6$ are the RSO and ground station's state vectors, respectively. P_d is the probability of detecting the space object in a given image. The function f represents whether or not an RSO is in the field-of-view (FoV) of the ground station and is detectable by the sensor.

The initial (prior) BPA for a particular hypothesis h is denoted $m_{h,0}$. A challenging aspect of this work is mapping pieces of evidence to hypotheses and forming BPAs that can be combined using Dempster's combination rule. Generally, for a particular hypothesis Θ_h, Dempster's combination rule results in a final BPA for hypothesis h:

$$m_{h,\alpha} = m_{h,0} \oplus m_{h,ev_1} \oplus ... \oplus m_{h,ev_i} \oplus ... \oplus m_{h,ev_E} = m_{h,0} \oplus \bigoplus_{i=1}^{E} m_{h,ev_i}, \tag{12}$$

where m_{h,ev_i} are evidence BPAs acquired at time-step t_i related to hypothesis h. E is the total number of acquired pieces of evidence. Multiple pieces of evidence can be gathered at a single time index if multiple sensors are used. As such, the pieces of evidence result from selecting a given sequence in α. Not every hypothesis state will be updated at each time-step. This highlights the need for an effective decision-making algorithm, since taking an action over another always results in some opportunity cost.

Since optimizing Eqn. 10 is non-trivial, the original formulation is broken down into a sub-problem using adversarial optimization for computational tractability. An action tree is formed and optimized by using alpha-beta pruning. An alternating agent approach is adopted using minimax and maximin optimization. In minimax optimization, both agents try to minimize the potential loss for a worst-case scenario. Similarly, in maximin optimization, both agents try to maximize their minimum gain.

A pair of agents are assigned to each proposition $\{\theta\}$ for every hypothesis Θ_h. In the case of binary hypotheses, only a single pair is assigned to the frame, since the critic agent would try to minimize the belief in $\{\theta\}$. This transforms part of the action-sequence computation into an alternating turn game. By finding and implementing action sequences that are proposition selfish, one gives equal opportunity to opposing agents to build a case for or against a particular proposition. This process is analogous to the judicial system, where two sides build a case with supporting evidence, hence the name Judicial Evidential Reasoning. This approach reduces confirmation bias and limits convergence to erroneous propositions. For this purpose, the JER algorithm iteratively flips between maximin and minimax optimization.

For a particular hypothesis $\Theta_h \in \Theta$, each proposition must be confirmed or refuted with evidence, so each proposition is assigned a pair of agents. When the advocate agent is active, its goal is to maximize belief in proposition $\{\theta\}$, using maximin optimization with the plausibility transform:

$$\alpha^*_{\{\theta\}} = \arg\max_{\alpha} \min \quad Pr_{pl}(\theta; m_{h,\alpha}), \quad \{\theta\} \in 2^{\Theta_h}, \tag{13}$$

where $m_{h,\alpha}$ is the final BPA for hypothesis h as a result of implementing action sequence α. The plausibility probability is maximized when $m(\{\theta\}) = 1$ and is minimized when $m(\{\theta\}) = 0$. When the critic agent is active, its goal is to maximize belief in $\neg\theta$ or equivalently, minimize belief in $\{\theta\}$, thus the formulation flips to:

$$\alpha^*_{\neg\theta} = \arg\min_{\alpha} \max \quad Pr_{pl}(\theta; m_{h,\alpha}),\ \neg\theta \in 2^{\Theta_h} \tag{14}$$

The set of all proposition minimax or maximin action sequences, $\alpha^*_{\{\theta\}}$ and $\alpha^*_{\neg\theta}$, is denoted α_{agents}. Once the agent pairs have evaluated the maximin or minimax action sequences for each

proposition, a final action sequence needs to be chosen from the full set of possible maximin or minimax actions α_{agents}. This is done by determining which sequence in α_{agents} minimizes the original cost function:

$$\tilde{\alpha}^* = \underset{\alpha_{agents}}{\arg\min} \sum_{h=1}^{|\Theta|} w_h H_{JS} \tag{15}$$

To capture the changing belief states over time, the JER algorithm is implemented using a receding time-horizon approach. Consequently, the first actions in $\tilde{\alpha}^*$ are implemented and the full process is repeated again for the next time step. The actions change the belief state initial conditions, providing the necessary feedback for the algorithm to resolve all of the hypotheses. More details regarding JER can be seen in Jaunzemis' prior work.[7] JER does require significant computational effort, due to the lack of analytical optimality conditions, as mentioned above. Many action sequence combinations are evaluated. The problem size grows exponentially with increasing numbers of hypotheses. To compensate for this limitation, alpha-beta pruning is used to prune suboptimal minimax or maximin actions in the decision trees.

JER and SSA Applications

Satellite operators and monitors are interested in whether RSOs are in their nominal orbits. An object can be in an anomalous orbit if force perturbations act on the body over time or the object performs a maneuver, resulting in deviations away from the nominal trajectory. Both of these cases can result in a loss of custody. Maintaining custody of objects is pivotal to prevent conjunction events or collisions. As such, these hypotheses are investigated in this paper for a set of RSOs.

The geometry of the problem is shown in Figure 1. The telescope's FoV will determine how many distinct actions are required. If multiple objects of interest can be seen in one image, less independent actions are required to resolve their hypotheses. The available telescope actions are abstracted as "track" or "search" actions. The action length is fixed and uniform throughout the whole time-horizon. The "track" action results in the telescope observing the nominal TLE trajectory for an RSO over the action interval. The "search" action performs a reachability set search around the nominal trajectory. In Figure 1, there is a single ground station and three RSOs in the ground station's FoV. Since the telescope cannot observe all of the RSOs simultaneously, JER computes when each RSO is observed. In the illustration, two RSOs are in nominal orbits that closely match the TLE. One object has maneuvered and is deviating significantly from the nominal trajectory.

Figure 2 provides a visual explanation of a case where an anomaly has occurred. As observations of the satellite are acquired, the estimated state will converge towards the truth. As time elapses, the dissimilarity of the trajectories becomes increasingly obvious. If observations were taken near the epoch time t_0, there could be some ambiguity regarding the orbit status, due to the trajectories' proximity and high estimate covariance. However, if the same process is repeated later, closer to t_f, it becomes more obvious that the RSO is anomalous. In practice, when this divergence becomes significant enough is not known a-priori. As such, it is important to take repeated observations to gather an accumulation of evidence.

Using DS theory, the anomaly hypothesis is defined with the following frame of discernment:

$$\Theta_A = \{\mathcal{N}, \mathcal{A}\}, \tag{16}$$

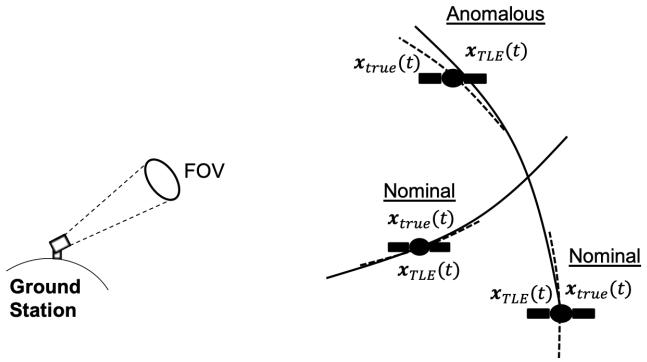

Figure 1: Geometry of the Problem

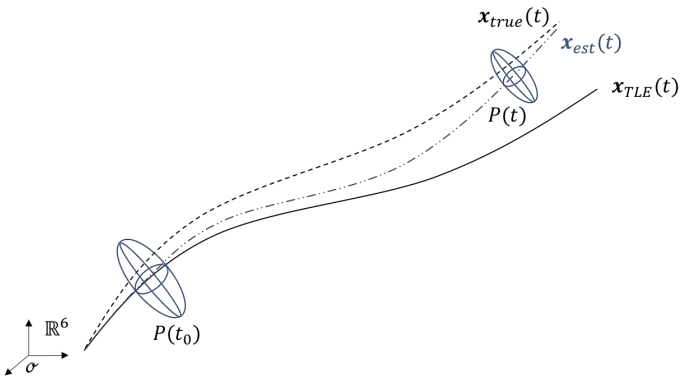

Figure 2: Anomaly Illustration

where $\mathcal{N}$ and $\mathcal{A}$ denotes nominal and anomalous, respectively. The power set of the frame is:

$$2^{\Theta_A} = \{\emptyset, \{\mathcal{N}\}, \{\mathcal{A}\}, \{\mathcal{N}, \mathcal{A}\}\} \tag{17}$$

Similarly, the custody frame of discernment is:

$$\Theta_C = \{C, \neg C\} \tag{18}$$

and the corresponding power set is:

$$2^{\Theta_C} = \{\emptyset, \{\mathcal{C}\}, \{\neg\mathcal{C}\}, \{\mathcal{C}, \neg\mathcal{C}\}\} \tag{19}$$

The evidence acquired over an action interval is defined by the following BPAs:

$$
\begin{aligned}
m_c(\{C\}) &= P_d * P_c * K_c \\
m_c(\{\neg C\}) &= P_d * (1 - P_c) * K_c \\
m_c(\Theta_C) &= 1 - m_c(\{C\}) - m_c(\{\neg C\}) \\
m_a(\{N\}) &= P_d * P_n * K_n \\
m_a(\{A\}) &= P_d * (1 - P_n) * K_n \\
m_a(\Theta_A) &= 1 - m_a(\{N\}) - m_a(\{A\})
\end{aligned}, \tag{20}
$$

where P_d, P_c, and P_n are the probability of detecting an RSO in a given image, the probability of having custody, and the probability of an RSO being nominal, respectively. The scalars K_c and K_n are defined between $[0, 1]$. If they are less than 1, they provide belief mass to the frame of discernment as ambiguity. This is used in this work to acquire multiple pieces of evidence to achieve proper hypothesis resolution.

RSO state estimates are obtained using an Unscented Kalman Filter (UKF) and angles-only measurement updates,[15] resulting from processed images. It is assumed that the multi-dimensional state distribution of the RSO is Gaussian, with mean $\hat{\mathbf{x}}$ and covariance P:

$$
\mathbf{x} \sim \mathcal{N}(\hat{\mathbf{x}}, P) \tag{21}
$$

The probability of an RSO being nominal, P_n, is computed using the Mahalanobis distance (MD) between a state estimate, $\hat{\mathbf{x}}$, and the nominal state from the propagated TLE trajectory, $\mathbf{x}_{TLE}$. The relevant MD is computed as:

$$
d(\mathbf{x}_{TLE}) = \sqrt{(\mathbf{x}_{TLE} - \hat{\mathbf{x}})^T \tilde{P}^{-1} (\mathbf{x}_{TLE} - \hat{\mathbf{x}})} \quad \mathbf{x}_{TLE}, \hat{\mathbf{x}} \in \mathbb{R}^6 \tag{22}
$$

The MD is a measure of the probability that $\mathbf{x}_{TLE}$ belongs to the distribution:

$$
\mathbf{x} \sim \mathcal{N}(\hat{\mathbf{x}}, \tilde{P}), \tag{23}
$$

Where,

$$
\tilde{P} \neq P \tag{24}
$$

The distance matrix $\tilde{P}$ used is not the estimate's covariance matrix. If an estimate converges towards the truth and has a "small" covariance, then large MD can be computed despite true proximity in state space, yielding an RSO to be erroneously classified as anomalous. As such, to better classify the anomaly, $\tilde{P}$ is defined a-priori as a region around the state estimate mean such that if $\mathbf{x}_{TLE}$ falls within this region, it is likely to be considered nominal. The matrix $\tilde{P}$ is defined as:

$$
\tilde{P} = diag(\tilde{\sigma}_x, \tilde{\sigma}_y, \tilde{\sigma_z}, \tilde{\sigma}_{\dot{x}}, \tilde{\sigma}_{\dot{y}}, \tilde{\sigma}_{\dot{z}}), \tag{25}
$$

where,

$$\tilde{\sigma}_i = \frac{20}{\sqrt{3}}\, km,\ \ i = x, y, z \tag{26}$$

$$\tilde{\sigma}_k = \frac{0.2}{\sqrt{3}}\, km/s,\ j = \dot{x}, \dot{y}, \dot{z} \tag{27}$$

These conservative values are chosen because of the instrumentation used, the location of the ground station, and since unmodeled perturbations can induce deviations of roughly 10 km per day for satellites in geostationary orbits.

Moreover, let Q be a random variable, representing the squared MD, with chi-squared distribution:

$$Q \sim \chi^2(k), \tag{28}$$

where k are the degrees of freedom of the distribution, equal to the dimension of the vector $\mathbf{x}_{TLE}$

$$k = dim(\mathbf{x}_{TLE}) = 6, \quad \mathbf{x}_{TLE} \in \mathbb{R}^6 \tag{29}$$

As such, to quantify anomaly, the question can be posed by speculating whether the vector $\mathbf{x}_{TLE}$ belongs to the distribution given by $\mathcal{N}(\hat{\mathbf{x}}, \tilde{P})$. This is the same as detecting outliers using the MD of a given point with respect to some mean. The probability that $\mathbf{x}_{TLE}$ belongs to the underlying distribution is then:

$$\mathcal{P}(Q > d^2(\mathbf{x}_{TLE})) = 1 - \mathcal{P}(Q \leq d^2(\mathbf{x}_{TLE})) \tag{30}$$

This probability is readily computed using statistical packages. Thus, the probability that an object is in the nominal orbit is given by:

$$P_n = \mathcal{P}(Q > d^2_{\mathbf{x}_{TLE}}) \leq 1 \tag{31}$$

The higher the MD, the lower P_n, providing more support to the anomalous proposition of an RSO's frame of discernment.

The approach used to compute P_c, the probability of having maintained custody, is simpler. If an action to track a particular RSO is taken, and the RSO does not appear in the FoV, then there may be evidence of lost custody. Hence, a thresholding technique is used based on whether the RSO is detected, yielding:

$$P_c = \begin{cases} 0, & Not\ Detected \\ 1, & Detected \end{cases} \tag{32}$$

The probability of detecting an RSO in optical data, P_d, scales the belief masses in the singleton propositions of the hypotheses. It is defined in Coder et. al's prior work.[16] In general, it is a function of telescope parameters, atmospheric transmittance, sky brightness, and the detection algorithm used. Environmental effects can alter the visibility of an object in optical data, which in turn alter

how the evidence being fed into JER is quantified. High probability of detection should minimally impact the evidence for a proposition. However, low probability of detection would imply more ambiguity in the measurements obtained, and thus, should reduce the belief mass given to a proposition. In practice, the demonstration is only attempted on cases where the probability of detection was high due to clear skies and thus P_d is kept constant in the current work.

If the belief in the custody proposition increases past a certain threshold, a search action has to be taken to find the RSO and maintain custody of it again. This assumption constrains the reachable distance of an RSO relative to the nominal orbit. Since reachability set searches are not the focus of this paper, a simplification is made regarding the maximum distance of the reachable set based on a Lemma in Holzinger et. al's previous work.[17]

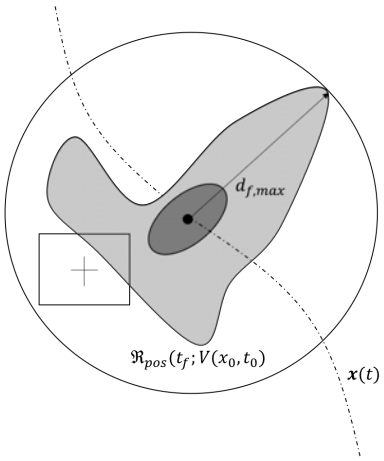

Figure 3: Reachable Volume Search

The reachable set, $\mathcal{R}_{pos}$ is pictured in Figure 3. The exact reachable set can be seen by the larger gray volume. For an arbitrary initial ellipsoidal surface, there is a maximum reachable distance in a given time-horizon. Instead of assuming some control thrust capability for each RSO, this paper assumes a conservative $d_{f,max}$ of 155 km, or an angular error of $0.25°$. The rectangle in Figure 3 represents the telescope's FoV in Cartesian state space or the projection of state space onto the telescope's image plane. When searching the state space, images are taken sequentially over this volume. The maximal spherical volume in $\mathbb{R}^3$, with radius $d_{f,max}$, is projected onto the image plane and then the area is divided into angular coordinates. These sub-areas of the projected volume are observed until the RSO of interest is detected and tracked, so that custody is maintained again by updating the state estimator. The search volume, projected into angular space, results in:

$$\begin{aligned} \alpha_{max,min} &= \alpha_{est} \pm \phi_d \\ \delta_{max,min} &= \delta_{est} \pm \phi_d \end{aligned} \tag{33}$$

Where ϕ_d is the maximum angular offset to search in angle space, corresponding to the reachability radius $d_{f,max}$. Additionally, $\alpha_{est}, \delta_{est}$ are the estimated topocentric right-ascension and declination of an RSO.

HARDWARE & EMPIRICAL METHODOLOGY

The JER algorithm is fundamentally a scheduler, telling each sensor in a network what RSO to observe. Adversarial optimization is used to compute agent schedules, which are combined to form an aggregate schedule that best reduces system entropy. A summarized process highlighting the JER algorithm for the empirical validation is presented in Algorithm 1. The receding horizon approach results in the first action being selected and executed. The measurements over an action interval are used to quantify the evidence. A BPA is formed for each piece of evidence, which are then combined, updating the belief states for each hypothesis. This process is repeated until the overall J-S entropy is reduced below some predefined threshold.

Initialize:
Ground stations;
UKF estimators;
Reachability volume;
D-S Hypotheses;
while $\sum_{h=1}^{|\Theta|} w_h H_{JS} > H_t$ *and* $t_i < t_f$ **do**
- Compute action sequences: adversarial agent optimization & $\alpha - \beta$ pruning;
- Form agent combination schedules α_{agents};
- Compute optimal aggregate schedule, $\tilde{\alpha}^*$, that minimizes $\sum_{k=1}^{|\Theta|} w_k H_{JS}$;
- Execute first action: capture and process images (evidence);
- Fuse evidence and update hypotheses Θ: Dempster's Combination Rule

if *Lost custody:* $m(\{\neg C\})_h > t_c$ **then**
  Trigger reachability set search;
else
  Continue with nominal RSO observations ;
end
end

Algorithm 1: Judicial Evidential Reasoning Algorithm Summary

A sophisticated code base is required to communicate with the telescope mount and electro-optical sensors simultaneously. For this particular trial, GT-SORT, located in Midtown, Atlanta, USA, is used. This high-resolution and narrow FoV Raven Class telescope is made with commercially-off-the-shelf components. Software Bisque's Paramount ME II telescope mount is used to control the pointing with TheSkyX Professional Edition software. Interfacing the JER code and incorporating telescope and camera control modules requires custom made scripts developed in Python. Two optical sensors are used, namely, the ZWO AS I071MC Pro (color) and ZWO ASI174MM-Cool (mono) cameras. The cameras are used for the telescope and finder scope, respectively. The physical setup used is detailed in Figure 4 and Figure 18 in Appendix A.

The images taken with the main telescope and finder scope cameras are processed and used to quantify evidence as described above. To extract accurate measurements, calibration is required to remove sources of error in the hardware setup using a telescope T-Point model. The effect of timing errors are mitigated during the data acquisition phase by synchronizing the main computer's clock

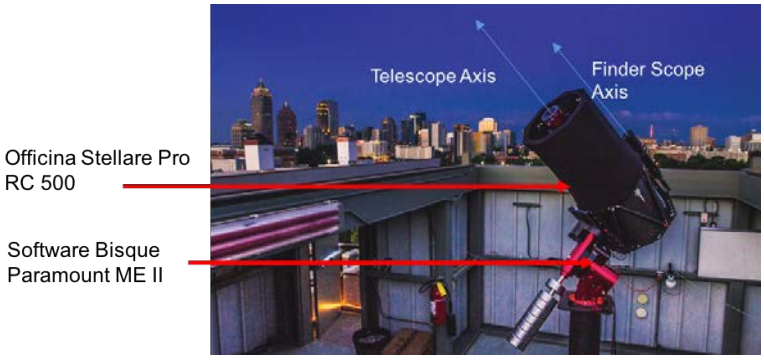

Figure 4: GT-SORT Ready to Track Space Objects from Midtown Atlanta, USA

with atomic clocks through a Network Time Protocol (NTP) server. Additionally, the finder scope's bore sight is aligned with the main telescope's optical axis by observing and adjusting the finder scope mount after pointing at a particular star or feature with both cameras. Table 1 and 2 shows the GT-SORT and finder scope optical performance characteristics.

Table 1: GT-SORT Performance

Focal Ratio	FoV (arcmin.)	iFoV (arcsec.)	Limiting Magnitude
f/6	25.56 x 16.98	0.31	12.9

Table 2: Finder Scope - Rokinon 135 mm Lens - Performance

Focal Ratio	FoV (arcmin.)	iFoV (arcsec.)	Limiting Magnitude
f/2	287.58 x 181.38	8.127	12.06

Since the GT-SORT takes high-angular resolution and narrow FoV images, detecting stars in a location like Midtown Atlanta, with high amounts of light pollution, is difficult. Answering the anomaly hypothesis requires rate-tracking an RSO and acquiring accurate astrometric information from the images. The light pollution in the city makes star detection challenging with narrow FoV telescopes. Additionally, to identify the object in a given image, multiple images have to be processed for successful object discrimination. When the telescope is rate-tracking a TLE, the RSO's position will remain approximately in the same pixel coordinates with the addition of some noise. Tracking the RSO frame to frame is done with a Gaussian-Mixture Probability Hypothesis Filter, readily available from previous lab projects. This is a high SNR multi-object tracking algorithm that uses multiple particle filters to track objects across several image frames.

To extract angle measurements, the inertial (star) background can be used to back out topocentric right ascension and declination measurements of the RSO. To compensate for a lack of star detections in the telescope's main camera, an additional wide FoV finder scope is used to extract more astrometric information. Figure 19, in Appendix A, shows the result of images taken with the finder scope and telescope simultaneously. The visible frame corresponds to the finder scope where the black detections are stars. The red detections are stars visible through the telescope mapped into

the finder scope's coordinate frame. The difference in angular FoV is evident in the figure. When rate-tracking, the number of star detections decreases significantly as the star point-spread functions (PSFs) are integrated over the sensor area in the telescope. Hence, using the finder scope increases the probability of resolving the astrometry of the image.

Using the two imaging systems requires mapping detections in one image coordinate system to another. This mapping can be subject to image distortion due to the telescope's FoV being much narrower than the finder scope's. First, the bore sights are aligned, so the detections in Figure 19, in Appendix A, will be centered. The telescope is pointed to an area near the RSOs location. Briefly, a static image is taken to compute the linear mapping registering the telescope's detections in the finder scope's FoV. Then, the telescope rate-tracks an RSO and captures images, obtaining astrometric information from the wide FoV sensor, and uses the a-priori defined mapping to obtain the corresponding right-ascension and declination for detections in the telescope image. This removes the need to run astrometry on the telescope images. Additionally, solving astrometry on the finder scope is faster due to increased star detections.

The mapping is assumed to be a linear transformation H, which can be identified using the telescope detections expressed in each frame's coordinate system as follows:

$$H \begin{bmatrix} x_1 & x_2 & ... & x_n \\ y_1 & y_2 & ... & y_n \\ 1 & 1 & ... & 1 \end{bmatrix}^{tele.} = \begin{bmatrix} x_1 & x_2 & ... & x_n \\ y_1 & y_2 & ... & y_n \\ 1 & 1 & ... & 1 \end{bmatrix}^{fin.} \tag{34}$$

Where the superscript on the right-hand side indicates the vectors are expressed in the finder scope's coordinate system. Thus, H maps telescope coordinates to finder scope coordinates. This operation, known as point-matching, uses least squares and the right-pseudo inverse to form:

$$\begin{aligned} HQ &= P \\ H &= QP^T(PP^T)^{-1} \end{aligned} \tag{35}$$

The linear transformation H is then used to forego star detection in the telescope's images. The GM-PHD multi-object tracking algorithm is used to track RSOs in the telescope images, implemented in pixel-space. Once a measurement is obtained, the pixel-coordinates of the RSO are mapped to the finder scope's pixel coordinates. Since the finder scope image is solved with astrometry, the RSO's topocentric right-ascension and declination measurement is obtained. These measurements are fed to a UKF to update inertial position and velocity estimates of the RSO. These estimates need to be accurate enough to quantify the evidence for the anomaly hypothesis. Figure 5 shows the GM-PHD algorithm tracking ANIK G1 in a telescope image. The green dot is ANIK G1, the blue dots are other GEO satellites with similar pixel dynamics, and the red dots are streak detections. The corresponding finder scope image is visible in Figure 11, in Appendix A.

For the current implementation of JER, it is assumed that the object association problem, when updating the state estimator, has been correctly solved. A measurement gating approach is used to discriminate which measurements are used to update the RSO estimates.

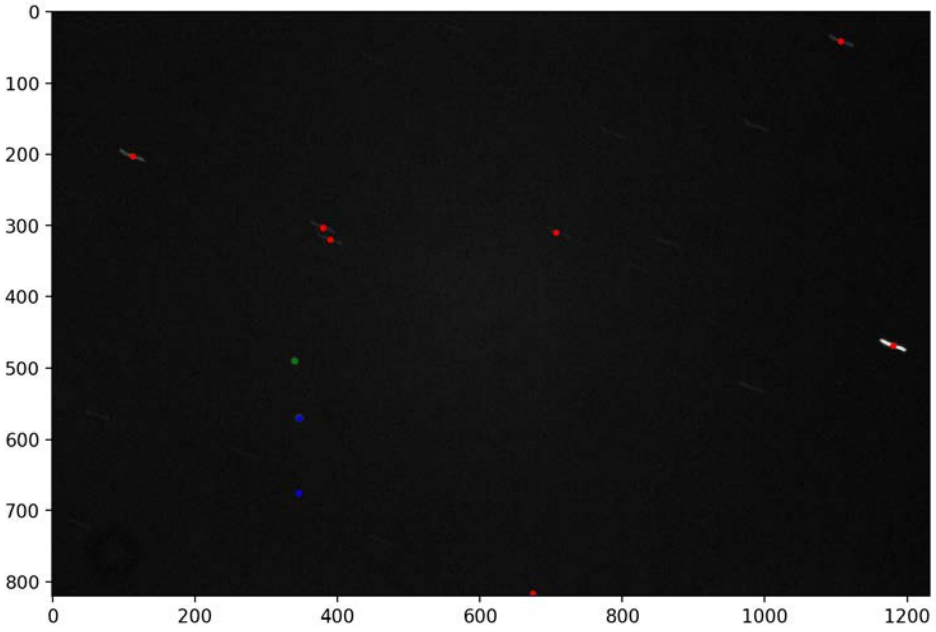

Figure 5: GM-PHD Tracking ANIK G1 - Oct. 31, 2018 2:08:03 UTC

SCENARIO DEFINITION

The main objective of this paper is to empirically validate and expand the JER algorithm's capabilities. The case and complexity to which JER is subjected relies heavily on the RSOs that are considered in the experiment. The empirical validation was posed to be challenging and relevant to the SSA community at large. Many important RSOs of interest lie in geostartionary Earth orbit (GEO) due their cost and impact on civil and commercial infrastructure. As such, a number of satellites in this orbital regime are considered.

A total of 3 GEO satellites are selected, namely, ANIK G1, ANIK F2, and GOES 14. GOES 14 performs East-West station keeping maneuvers only. ANIK F2 uses continuous thrust capabilities and ANIK G1 performs North-South and East-West station keeping. These three objects are active and use different kinds of maneuvers periodically, which makes them suitable objects to consider for the anomaly and custody hypotheses. Additionally, the 3 GEO satellites adequately represent the broader GEO satellite population, and are thus good candidates for validating the presented tasking approach.

RESULTS

The obtained results are from an observation campaign on Oct. 30, 2018, during Atlanta's GEO glint season, providing adequate conditions to detect and track GEO satellites. A time-horizon of two hours is given to the JER algorithm, though the algorithm was able to resolve the hypotheses in less than an hour. The action intervals were fixed and 3 minutes long. A total of 16 actions were taken in the demonstration, totaling up to 48 minutes of observation time. Every satellite was resolved as nominal since the deviations with respect to their nominal TLE trajectories were small in magnitude. Though the objective of the JER approach is not to minimize the covariance of the

satellite estimates, the estimates do need to be accurate enough to quantify the anomaly and custody related evidence. This constrains the telescope action interval duration such that measurement updates reduce the overall estimate covariance.

Table 3 shows the deviation of the state estimates with respect to the TLE nominal states at the final time of the demonstration. It can be seen that ANIK G1 and GOES 14 are very close to the nominal trajectory, off by 4.17 and 3.19 km, respectively. This is expected given that the TLE was updated that day. Though the mean estimate for ANIK F2 deviated by 12.99 km in magnitude, since this deviation lies within the Gaussian region given by Eqn. 23, the RSO was resolved to be nominal. Table 3 also demonstrates that the differences between the nominal trajectory and estimated velocities are small, on the order of 10^{-4} and $10^{-5}km/s$, well inside the nominal region. The estimated state standard deviations can be seen in Figures 12 - 17 in Appendix A. These plots also show when the estimates of each RSO were updated along the time-horizon. The covariances decrease over time when measurement updates occur. Between observations, the integration of the process noise results in increased standard deviations. The final covariances are on the order of $10^{-1}km$ in inertial position and $10^{-4}km/s$ in inertial velocity.

Table 3: Estimate Deviation from TLE at Final Measurement Update

RSO	e_x km	e_y km	e_z km	$e_{\dot{x}}$ km/s	$e_{\dot{y}}$ km/s	$e_{\dot{z}}$ km/s
ANIK G1	1.206	0.9063	3.889	-2.056E-4	-2.037E-4	6.909E-4
ANIK F2	0.066	2.299	-12.794	-1.266E-4	4.774E-5	-1.540E-4
GOES 14	0.521	1.473	-2.781	-1.327E-4	-1.344E-4	-4.4356E-5

The receding-horizon optimal schedule that the JER algorithm commanded is visible in Figure 6. At the beginning of each action time, JER solves for the optimal sequence and implements the actions visible in the schedule. All of the actions commanded the telescope to "track" the nominal trajectories of the corresponding RSOs. Each tab indicates a single action taken by the GT-SORT. All of the RSOs were observable and visible since they did not enter the Earth's shadow.

In Figure 6, the blue rectangles indicate that the telescope was idle for those particular time-steps. As mentioned in the previous section, future JER action sequences are contingent on the evidence received and on the resulting BPAs formed. As such, it is iterative and the evidence provides feedback to the algorithm on how to minimize the total entropy of the frames of discernment. This schedule plot shows how the JER algorithm switches back and forth between the 3 GEO satellites. After roughly 48 minutes, the hypotheses are resolved and therefore the telescope becomes idle. Since the belief in any of the custody hypothesis never increased beyond the threshold, no reachability set search was triggered for this case.

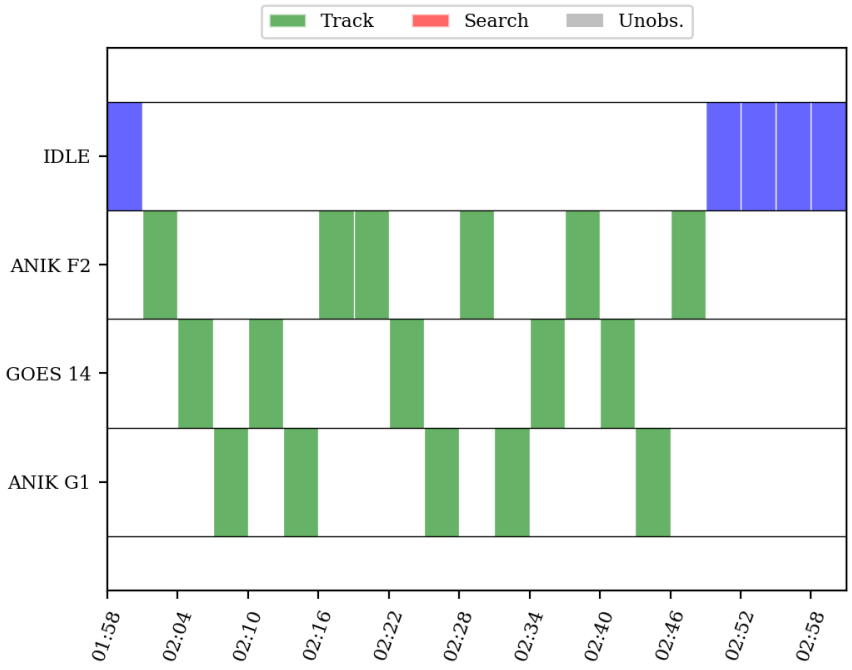

Figure 6: GTSORT Optimal Action Sequence (Schedule)

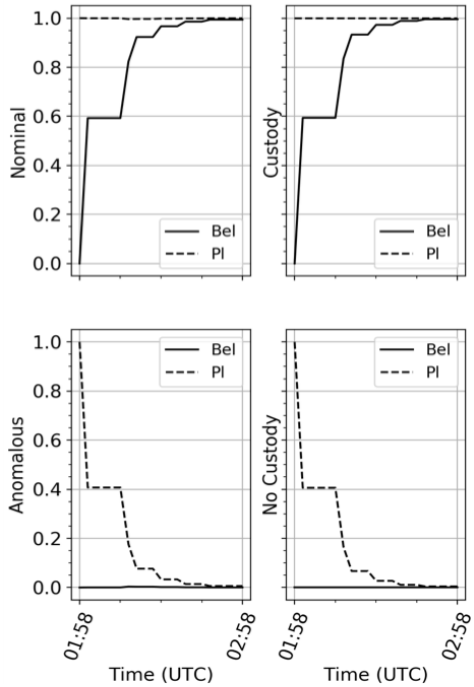

Figure 7: ANIK F2 Belief and Plausibility vs. Time

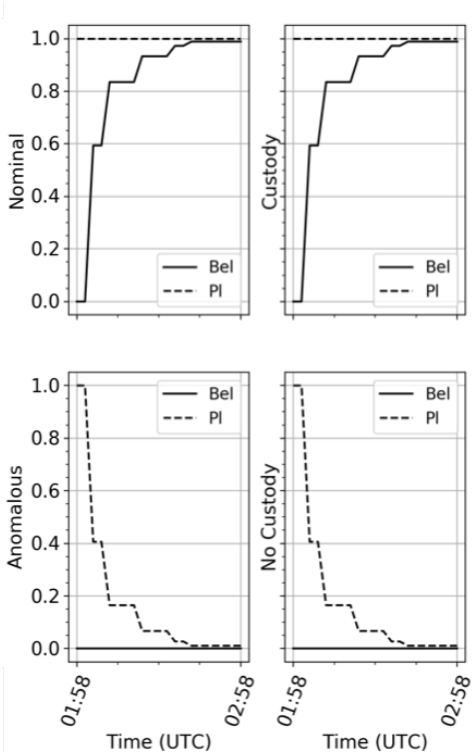

Figure 8: GOES 14 Belief and Plausibility vs. Time

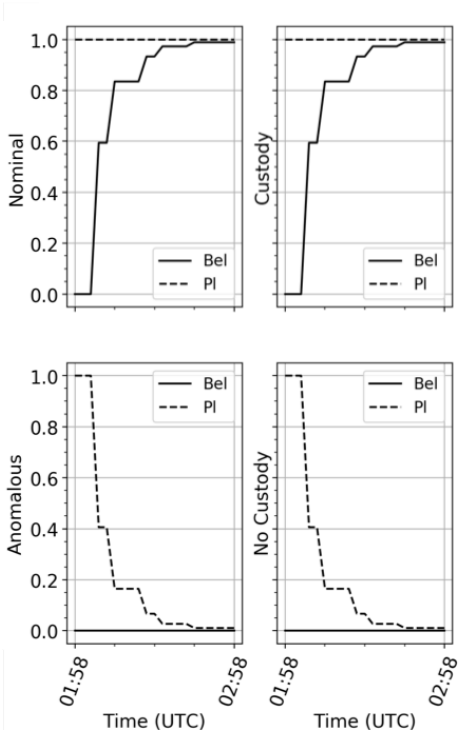

Figure 9: ANIK G1 Belief and Plausibility vs. Time

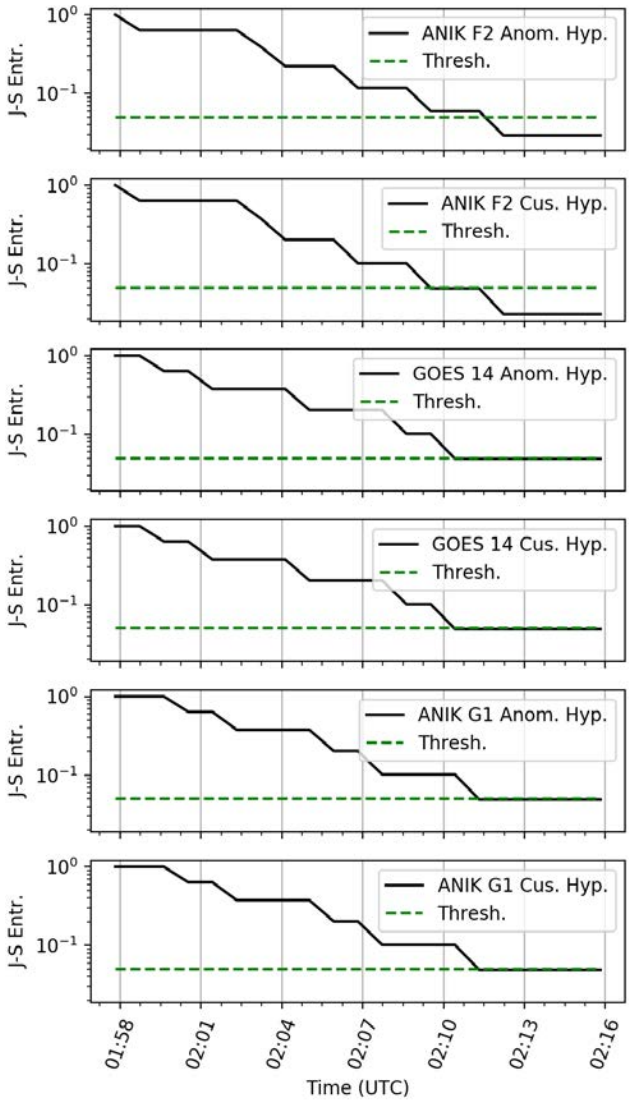

Figure 10: J-S Entropies Over Time

The information contained in the resulting BPAs are visible in Figures 7 - 8. The singleton propositions of the frames of discernment are visible along the y-axis of each subplot. The belief and plausibility of each proposition over time can be seen for each RSO in the experiment. Belief and plausibility can be interpreted as the lower and upper bounds of a proposition's probability. As the belief in the nominal and custody hypotheses increases for all of the RSOs, the plausibility of the propositions remains 1. The lower bound effectively increases until it meets the upper bound, resulting in hypothesis resolution. Conversely, the degree of belief (or support) in the anomalous and no custody propositions remains zero for the whole interval since no evidence is gathered that supports those propositions. Increasing belief in the nominal and custody propositions results in decreased plausibility of the anomalous or no custody hypotheses, which is evident for every RSO.

As the belief in a particular proposition of the frame of discernment increases, the J-S entropy is

expected to decrease, since the hypotheses are incrementally being resolved. The total uncertainty in the system, in terms of conflict and non-specificity, is being driven to zero. This suggests that a BPAs belief mass is increasingly being given to a singleton proposition in the frames of discernment, which is directly equivalent to resolving (answering) the hypothesis. This is also visible in Figure 10, which shows how the entropies of each hypothesis decrease over time. The solid black line is the J-S entropy of each hypothesis and the dashed green line represents the acceptable resolution threshold for the experiment. Naturally, all of entropies for the custody and anomaly hypotheses of each RSO decay below the resolution threshold, set at 0.05. The entropies of each hypothesis decrease at different times as a result of actions being taken for each RSO at different times.

CONCLUSION

This paper presented an application and extension of the JER by considering the custody and anomaly hypotheses and interfacing the algorithm with the GT-SORT. A reachability search action was incorporated into the algorithm in case there was a loss of custody of an object. A robust telescope mount controller, UKF estimator, and GM-PHD object tracking algorithm are implemented to resolve the anomaly and custody hypotheses correctly. An empirical validation was completed using 3 GEO satellites in real-time on October 30, 2018. Custody was maintained and the anomaly hypotheses were resolved as nominal for all of the investigated RSOs. The predictive JER sensor tasking algorithm successfully acquires and processes pieces of evidence using DS theory to resolve hypotheses in a timely manner. The results of this paper are promising and show a working proof of concept for hypothesis-based sensor tasking using evidential reasoning.

Future work includes handling a few limitations with the current framework. It is of interest to increase the number of objects that the algorithm can handle to better understand the algorithms quantitative capabilities. The algorithm also needs to be tested when abnormal behaviors are present to evaluate its ability to handle anomalies and false-alarm. Additionally, a 3D-axis attitude stabilized hypothesis will be incorporated in the future for particular RSOs. Another demonstration is planned with the proposed improvements in the first quarter of 2019.

REFERENCES

[1] T. Blake, M. Sánchez, J. Krassner, M. Georgen, and S. Sundbeck, "Space Domain Awareness," tech. rep., DEFENSE ADVANCED RESEARCH PROJECTS AGENCY ARLINGTON VA, 2012.

[2] R. S. Erwin, P. Albuquerque, S. K. Jayaweera, and I. Hussein, "Dynamic sensor tasking for space situational awareness," *American Control Conference (ACC), 2010*, IEEE, 2010, pp. 1153–1158.

[3] Z. Sunberg, S. Chakravorty, and R. Erwin, "Information space sensor tasking for Space Situational Awareness," *American Control Conference (ACC), 2014*, IEEE, 2014, pp. 79–84.

[4] K. Hill, P. Sydney, K. Hamada, R. Cortez, K. Luu, M. Jah, P. Schumacher, M. Coulman, J. Houchard, and D. Naho'olewa, "Covariance-based network tasking of optical sensors," *Paper AAS 10-150 presented at the AAS/AIAA Space Flight Mechanics Conference, February*, 2010, pp. 14–17.

[5] G. A. McIntyre and K. J. Hintz, "Information theoretic approach to sensor scheduling," *Signal Processing, Sensor Fusion, and Target Recognition V*, Vol. 2755, International Society for Optics and Photonics, 1996, pp. 304–313.

[6] R. Jiroušek and P. P. Shenoy, "Entropy of belief functions in the Dempster-Shafer theory: A new perspective," *International Conference on Belief Functions*, Springer, 2016, pp. 3–13.

[7] A. Jaunzemis, D. Minotra, M. J. Holzinger, K. M. Feigh, M. W. Chan, and P. P. Shenoy, "Judicial Evidential Reasoning for Decision Support Applied to Orbit Insertion Failure," *1st International Conference on Space Situational Awareness*, IAA, 2017.

[8] A. D. Jaunzemis, M. J. Holzinger, and K. K. Luu, "Sensor tasking for spacecraft custody maintenance and anomaly detection using evidential reasoning," *Journal of Aerospace Information Systems*, Vol. 15, No. 3, 2018, pp. 131–156.

[9] G. Shafer, *A mathematical theory of evidence*, Vol. 42. Princeton university press, 1976.

[10] D. Ellsberg, "Risk, ambiguity, and the Savage axioms," *The quarterly journal of economics*, 1961, pp. 643–669.

[11] A. P. Dempster, "Upper and lower probabilities induced by a multivalued mapping," *Classic Works of the Dempster-Shafer Theory of Belief Functions*, pp. 57–72, Springer, 2008.

[12] B. R. Cobb and P. P. Shenoy, "On the plausibility transformation method for translating belief function models to probability models," 2006.

[13] J. J. Sudano, "Pignistic probability transforms for mixes of low-and high-probability events," *arXiv preprint arXiv:1505.07751*, 2015.

[14] R. Jiroušek and P. P. Shenoy, "A new definition of entropy of belief functions in the Dempster–Shafer theory," *International Journal of Approximate Reasoning*, Vol. 92, 2018, pp. 49–65.

[15] E. A. Wan and R. Van Der Merwe, "The unscented Kalman filter for nonlinear estimation," *Adaptive Systems for Signal Processing, Communications, and Control Symposium 2000. AS-SPCC. The IEEE 2000*, Ieee, 2000, pp. 153–158.

[16] R. D. Coder and M. J. Holzinger, "Multi-objective design of optical systems for space situational awareness," *Acta Astronautica*, Vol. 128, 2016, pp. 669–684.

[17] M. J. Holzinger and D. J. Scheeres, "Reachability results for nonlinear systems with ellipsoidal initial sets," *IEEE transactions on aerospace and electronic systems*, Vol. 48, No. 2, 2012, pp. 1583–1600.

APPENDIX A

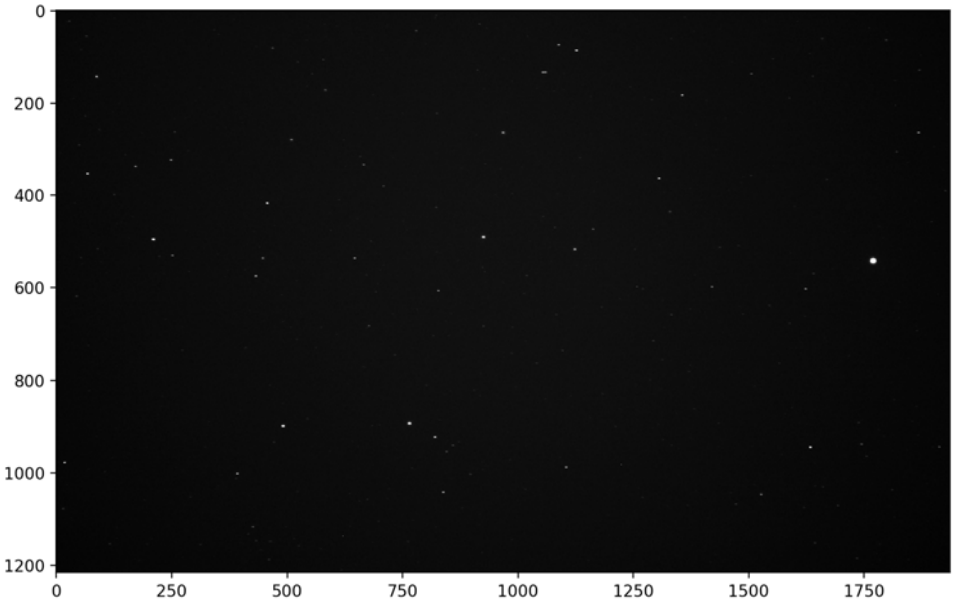

Figure 11: Sample Finder Scope Image Whilst Tracking ANIK G1

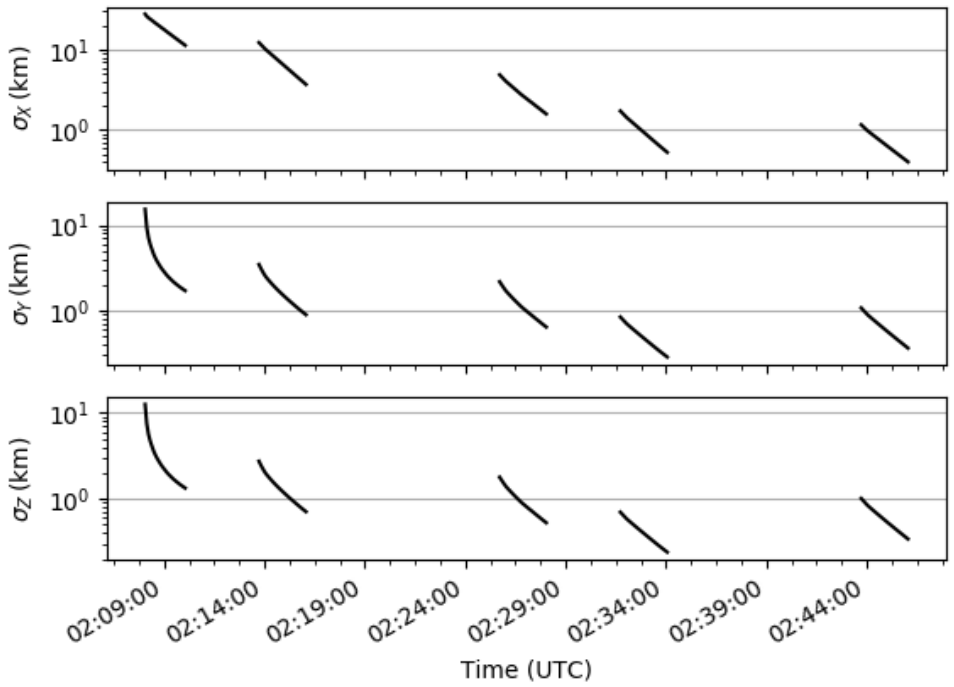

Figure 12: ANIK G1 Position Estimate Covariances

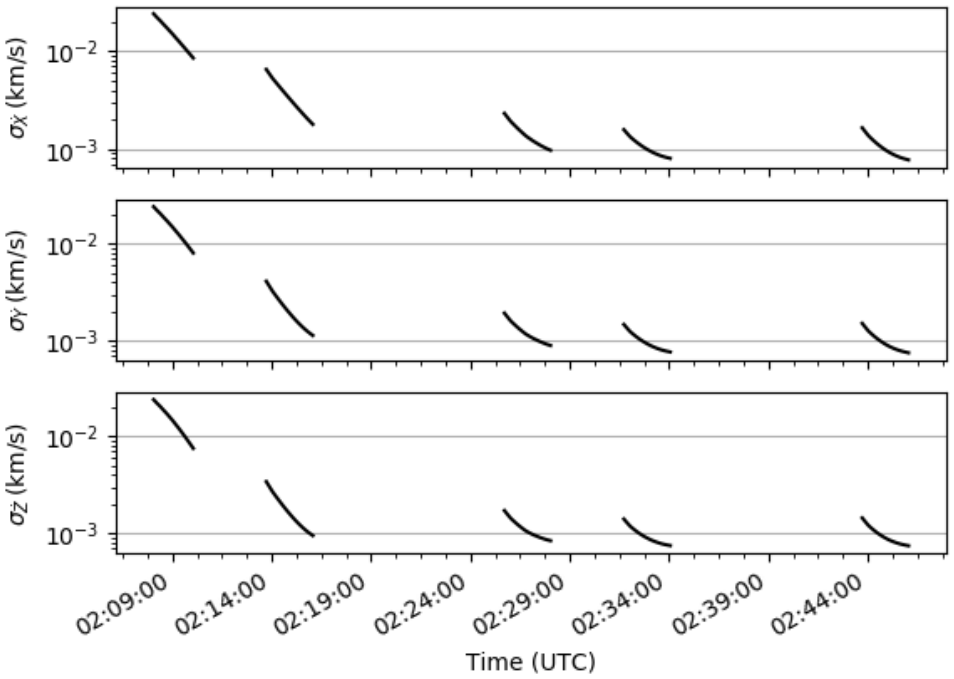

Figure 13: ANIK G1 Velocity Estimate Covariances

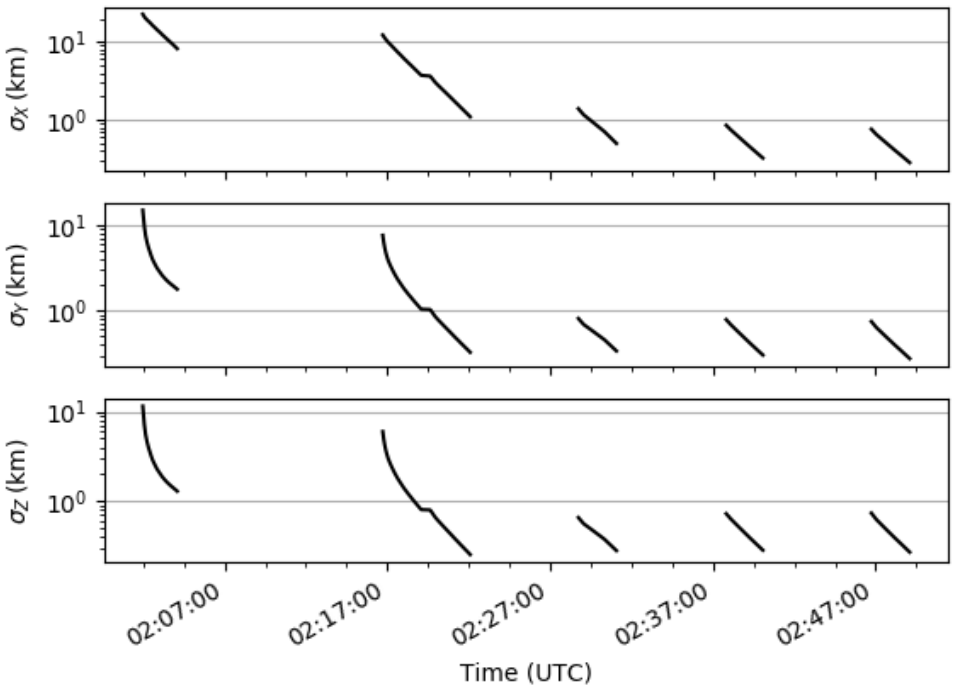

Figure 14: ANIK G1 Velocity Estimate Covariances

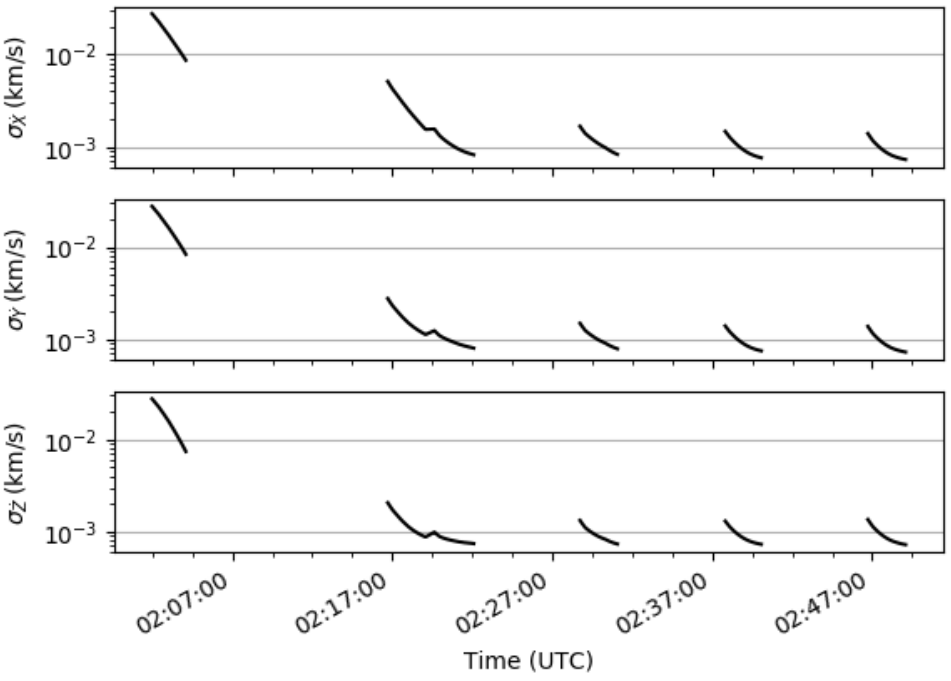

Figure 15: ANIK G1 Velocity Estimate Covariances

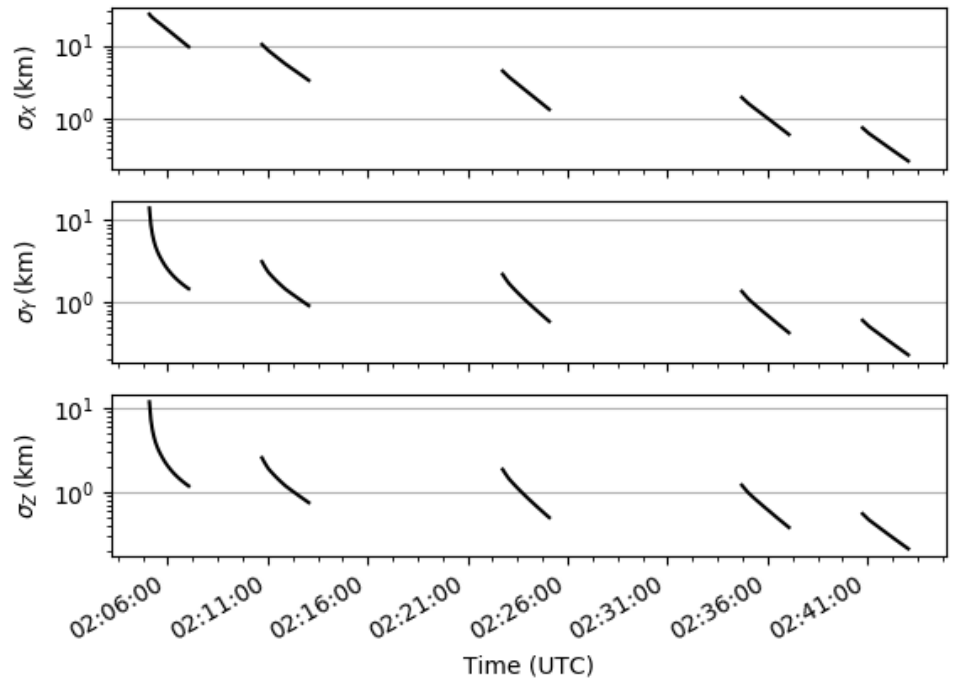

Figure 16: ANIK G1 Velocity Estimate Covariances

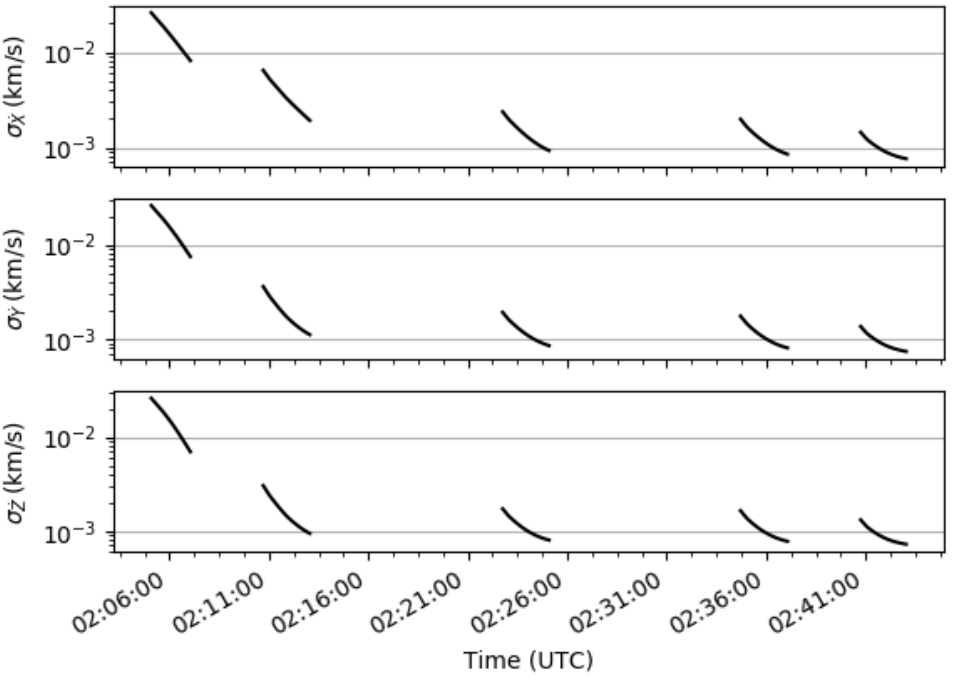

Figure 17: ANIK G1 Velocity Estimate Covariances

Figure 18: Rokinon Finder Scope

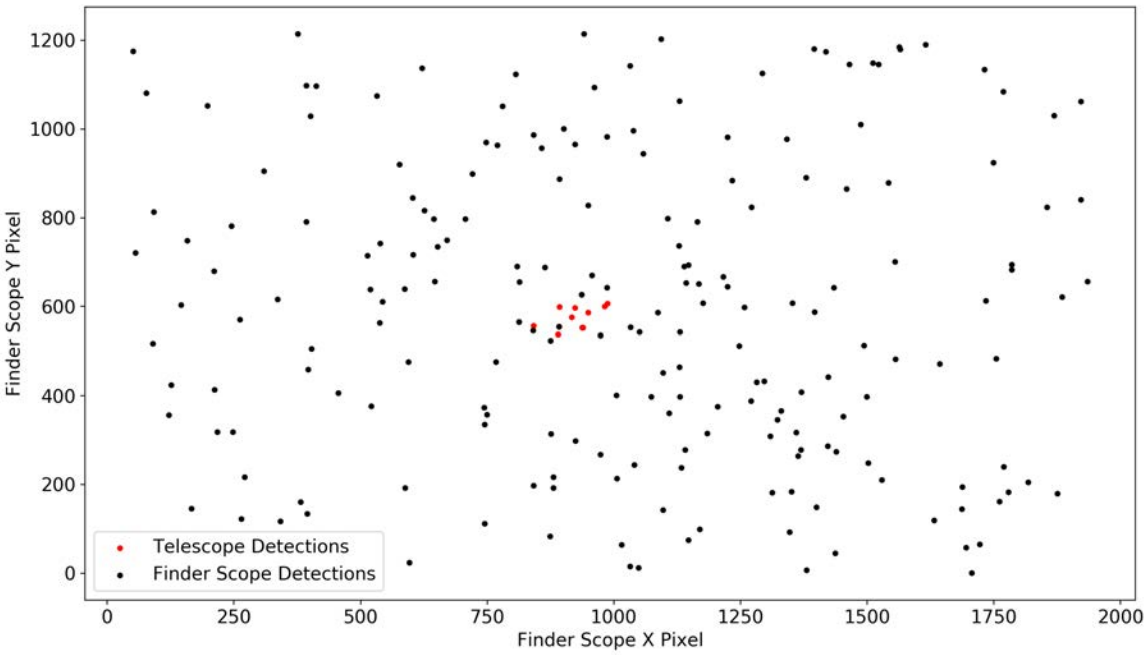

Figure 19: Object Registration in the Finderscope and Telescope